SEMARAK ILMU PUBLISHING

Journal of Advanced Research in Fluid Mechanics and Thermal Sciences

Journal homepage:
https://semarakilmu.com.my/journals/index.php/fluid_mechanics_thermal_sciences/index
ISSN: 2289-7879

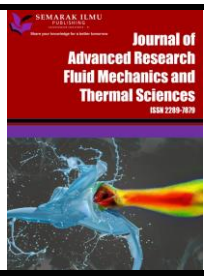

A Study into the Effect of Hull Configuration on the Performance of Floating Solar PV Structure

Mohammad Izzuddin Jifaturrohman[1], I Ketut Aria Pria Utama[2,*], Teguh Putranto[2], Dony Setyawan[2], Luofeng Huang[3]

[1] Department of Ocean Engineering, Faculty of Marine Technology, Institut Teknologi Sepuluh Nopember, Surabaya, 60111, Indonesia
[2] Department of Naval Architecture, Faculty of Marine Technology, Institut Teknologi Sepuluh Nopember, Surabaya, 60111, Indonesia
[3] Faculty of Engineering and Applied Sciences, Cranfield University, Cranfield, MK 43 0AL, United Kingdom

ARTICLE INFO

Article history:
Received 28 July 2024
Received in revised form 1 November 2024
Accepted 13 November 2024
Available online 30 November 2024

Keywords:
BEM; floating photovoltaic; monohull; renewable energy; seakeeping characteristics; twin hull

ABSTRACT

At present, energy transition is a reality in the journey towards achieving net zero emission. Among others, the development of floating solar photovoltaic (FPV) power plants is one of many possible renewable energy technologies that received considerable attention. One of the reasons for that is attributed to land acquisition which can lead to conflicts, whilst the use of sea is more flexible. Therefore, the development of floating solar PV situated at the near shore (later can be moved offshore) is promising particularly in order to withstand the harsh environment. The study aims to demonstrate such an innovative design of a floating structure and two types of hulls (monohull and twin-hull) are considered and focused on the seakeeping performance of the two bodies. BEM approach with Green-Function based on the 3-D diffraction panel method together with the use of the Joint North Sea Wave Project (JONSWAP) wave spectrum is carried out to accomplish the seakeeping characteristic. The final computational simulation results show that the twin-hull model has more advantages than the monohull design. The trend of the RAO pattern, response spectra, and significant response for heave and pitch motion represent only slight differences between the two proposed designs. However, substantial disparity emerges in roll motion, with the difference in response values in prevailing 0° -roll heading standing at 53%, 39%, 27%, and 18% for sea states 1 through 4, respectively. Moreover, in 45° wave heading (quartering sea) it demonstrates a slightly lower disparity compared to the 0° wave heading (following sea) through sea-state 1-4 standing for 50%, 37%, 24% and 16% respectively.

1. Introduction

Indonesia is determined to boost its use of renewable energy to approximately 10.72% of the national energy mix, aiming to reach 23% (equivalent to 10.6 GW) as outlined by the State Electricity Company (PLN) [1]. This plan retains a predominant reliance on coal (62.08%), natural gas (14.52%), and petroleum fuels. According to PLN, the expansion of hydroelectric and geothermal power plants is indispensable for meeting the 23% national energy mixed target since both can generate a

* *Corresponding author.*
E-mail address: kutama@its.ac.id

https://doi.org/10.37934/arfmts.124.2.124141

considerable amount of energy [2]. However, due to the challenges associated with land acquisition, environmental exploration, social issues, and a high investment value, these government projects have been frozen until now.

Initiative actions must be taken to explore alternatives to renewable energy resources. One example is the utilization of Floating Photovoltaic (FPV) technology. Over the last decade, extensive global research has been conducted on FPV technology, as detailed in previous studies [3-5]. This research includes various timelines for Floating PV projects, the global potential of FPV hybridized with hydropower, and several design solutions incorporating additional features such as tracking and cooling systems.

The World Bank has shown its attraction by publishing a book for practitioners interested in the field of FPV [6]. Subsequently, to ensure the safety design of FPV installation, DNV GL Class recommendations can be taken into consideration [7].

Ramasamy and Margolis [8] observed that the development of FPV technology is continuously growing, with China leading the way in 2020 by contributing 52% of the total 2.6 GW global installed capacity. Taiwan followed with 12%, Japan with 10%, Vietnam with 6%, South Korea with 5%, Netherlands, Israel, and India with 4% each and other countries contributed 3%. However, in the same year Indonesia started by partnering with Masdar [9] to implement FPV technology for the first time to generate 145 MW of power on a 250-hectare water area. With the successful previous project implementation of FPV, Indonesia collaborated with Sunseap commenced in 2021 on a 2.2 GW FPV project in the Batam Region [10].

Furthermore, several studies regarding the potential applications of FPV in Indonesia have been published. According to the Institute for Essential Services Reform (IESR) [11], approximately 42 of the water dam surface area in Central Java could generate up to 723.07 MWp of energy through FPV. The study by Joshi *et al.,* [12] suggests that, when fully optimizing the potential of all water dam surface areas across Indonesia, the power generation capacity could reach approximately 27.79 GWp. Supported by the highest potential Global Horizontal Irradiation (GHI) in Indonesia as informed by Ardiansyah and Ekadewi [13] within reaching up to 4.8 kWh/m^2 compared to other countries, it indicates that the application of FPV technology in Indonesia has significant and wide-open opportunities that require strategic planning for the future.

Within the design phase of an FPV system, a fundamental aspect is the floating structure component. This part is essential to ensure the system remains afloat and has enough buoyancy capacity. A study conducted by Sahu and Sudhakar [14] that typically the floating structure is made of non-hazardous, UV light-resistant, maintenance-free plastic materials with high tensile strength like High-Density Polyethylene (HDPE). However, there are other options such as concrete or steel proposed by Mittal *et al.,* [15] and Cazzaniga *et al.,* [16] respectively. Furthermore, Rosa-Clot and Tina [17] suggested that material selection for the floating structure shall consider several factors like modularity, flexibility, robustness, safety, sizing, and ease of launching technology to the site location.

Presently, HDPE blocks are predominantly employed in implementing FPV technology in lakes characterized by generally calm water conditions. These lakes are often surrounded by limited wind fetch, which minimizes wave generation and disturbance in the mountains-surrounded area as described well by Sigtryggsdottir [18] and Pullen *et al.,* [19]. Moreover, the effectiveness of FPV technology could be enhanced when deployed in near-shore locations and this represents an innovative leap forward due to open access in ocean space for a given greater technical area compared to installation over water dam surface area, which is restricted to only 5% of their total area based on Indonesia's Public Work and Housing regulation [11].

Additionally, Wang *et al.,* [20] presented that nearly 50% of the world's population resides within 100 kilometers of the coastline, positioning floating photovoltaic (FPV) systems as a promising solution to meet the growing energy demands of coastal regions. As these populations continue to expand as predicted by Kit *et al.,* [21], the consideration of FPVs as a sustainable energy source becomes increasingly important.

Due to this perspective, Liu *et al.,* [22] and Ahmed *et al.,* [23] presented that there are a few challenges that must be dealt with great external factors that impact the FPV system, such as wind-induced waves, current, seawater corrosion, biofouling, and long-term UV depreciation. An FPV structure must meet all environmental design requirements to keep the structure afloat and prevent capsizing.

Additionally, Andrady [24] emphasized that the problem of microplastic waste has become a major concern for marine ecosystems. Therefore, it is necessary to re-evaluate the use of HDPE on a large scale. Ciel & Terre [25] disclosed that the floater structure of FPV technology persists in the use of HDPE, which generally floats within a pin's connection type, which makes it ideal for places with insignificant wave heights (1 meter). The basic connection type of this HDPE floating structure is the weakest and most determines the strength system, so the area at this connection will be very sensitive to experiencing hot spots of stress concentration if there is an escalation in wave height from the design limit, resulting in the reliability of the structure in its operating area as stated by Oliveira-Pinto and Stokkermans [26].

Considering those various factors, there is a need to enhance the approach to developing the shape of PV technology floaters within certain study boundaries. This study introduces an innovative research gap performance that utilizes the geometric shape of steel hulls, offering the advantage of resilience to harsh marine environments and mitigating UV degradation effects. The effect of hull configuration as an initial design shall be evaluated under the JONSWAP wave spectrum using a BEM potential velocity theory-based simulation in various sea-state scenarios regarding both proposed designs with monohull and twin-hull floating platforms in correlated with stochastics approach for findings the external excitation motion.

The paper is organized as follows: in Section 2, the problem definition for the initial design of the floating hull structure is presented. Section 3 provides an overview of the research methodology and details the BEM numerical setup. Section 4 reports the results of a grid independence test conducted to evaluate the grid sensitivity used to discretize the computational domain of simulation results. Section 5 explains the BEM numerical simulation results and investigates the effect of hull configuration on motion characteristics. Finally, Section 6 offers a summary of the work along with its main conclusions.

2. Problem Definition

A single structure with a service deck of 36.00 m² areas could generate 3.99 kWp with 6 solar panels within 665 Wp capacity for each provided by CSI Solar [27], equivalent to the electricity demand of 3 households (HHs) which is estimated at around 200 Watts per HHs.

In ship design, the pivotal consideration of principal dimension ratios is related to crucial aspects such as longitudinal strength, ship manoeuvrability, cargo space, stability, and reserve buoyancy, as indicated in Table 1 below. These ratios are typically used for designed ships such as tankers, general cargo, bulk carriers, and/or high-speed vessels like the multihull concept. However, these ratios are neglected due to the stationary of the floater (non-propelled) and its exclusive purpose to provide buoyancy only.

Table 1
Main principal dimension ratios

Ratio	Twin-hull [28]	Monohull [29,30]	Correlation [29]
L/B	6.0 < L/B < 12.0	3.5 < L/B < 10.0	Ship manoeuvrability and cargo space
L/T	-	10.0 < L/T < 30.0	Longitudinal strength
B/T	1.0 < B/T < 3.0	1.8 < B/T < 5.0	Stability
T/H	-	0.7 < T/H < 0.8	Reserve buoyancy

The dominant pure oscillatory response motion of heave-, rolling-, and pitching characteristics in regular waves will be derived by examining the free-floating conditions of both proposed designs. The results will be presented in a Response Amplitude Operators (RAOs) graph, which will have the frequency parameter on the horizontal axis and the ratio of motion amplitude in a specific mode to the wave amplitude on the vertical axis as explained by Djatmiko [31].

3. Methodology

The numerical method utilizes the BEM simulation package in this study. The initial data of the main principal dimension, electricity demand, and weight calculation are presented in the subsection below, followed by a general arrangement. The seakeeping quality is determined by significant response spectra with stochastic calculation.

3.1 Model Description and Initial Calculation

The innovative initial design of floating PV structures, both single-hull and twin-hull for near-shore-based has been proposed as illustrated in Figure 1.

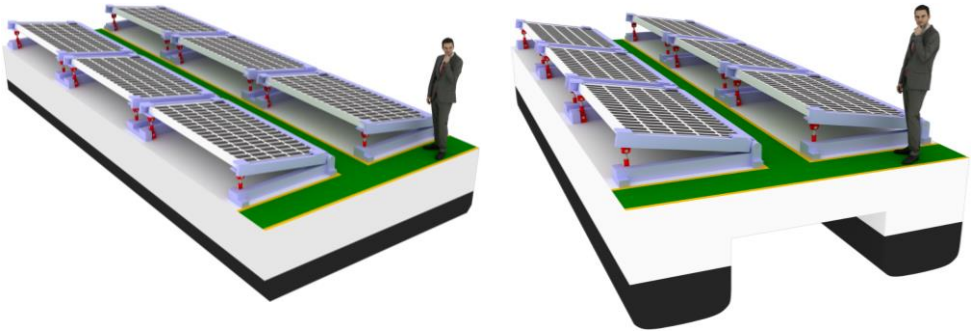

(a) (b)

Fig. 1. Initial proposed design: (a) Twin hull (b) Monohull

The main principal dimensions correlated with the hydrostatic properties of each design are tabulated in Table 2.

Table 2
Design main principal dimension

Parameter	Twin-hull	Monohull	Unit
Length Over All (LOA)	9.00	9.00	m
Breadth (B)	4.00	4.00	m
Height (H)	1.35	1.07	m
Draft (T)	0.53	0.25	m
Demihull Width (B1)	1.07	-	m
Spacing (S)	2.93	-	m
Hydrostatic properties			
Displacement (Δ)	9.96	9.13	ton
Block coefficient (C_B)	0.51	0.99	-
Prismatic coefficient (C_P)	0.99	1.00	-
Midship coefficient (C_M)	0.51	0.99	-
Keel to buoyancy (KB)	0.28	0.13	m
Longitudinal Center of Buoyancy (LCB) from AP	4.49	4.5	m

The general arrangement for both designs is illustrated in Figure 2. Walkway access is also considered with a width of 0.60 meters to provide space for maintenance purposes. the design of the tilt angle used a uniform 10 degrees for all panels relative to the stool at the main deck.

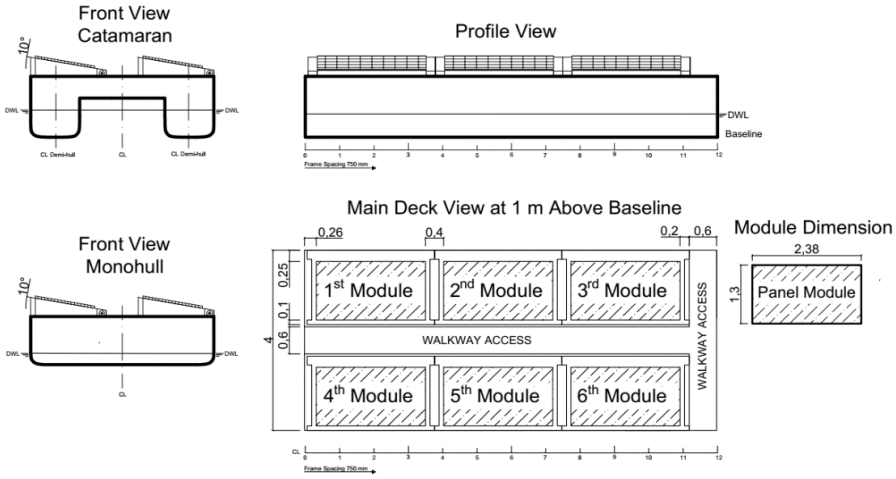

Fig. 2. General arrangement of the initial design of FPV

In addition, for electricity demand, topside weight and steel weight calculations are tabulated in Table 3. These initial calculations provided a global overview related to the selection of floaters for FPV technology. Nevertheless, this study shall be optimized in the future to improve design comprehension.

Table 3
Initial calculations

Parameter	Value	Unit	Remarks
FPV Electricity System			
PV capacity	665	Watt peak (Wp)	Canadian Solar Specification
Module efficiency	21.4	%	[27]
Length of PV	2.38	Meter	
Width of PV	1.30	Meter	
PV module weight	34.4	kg	
Irradiation	4.80	kWh/m^2	Ardiansyah and Ekadewi [13]
Electricity cons. Estimated per HH	200	Watt	
Time consumption	24	Hours	
Energy consumption per day	4.80	kWh	
System capacity included 25% of SF	1.25	kWp	Directorate General of Renewable Energy and Energy Conservation [32]
Number of PV needed	2	pcs	Per HH
Topside Weight Calculation			
Live Load for Operation & Maintenance (O&M)	400	kg	100 kg for each person assumption during O&M
Total Module Weight	206.40	kg	6 numbers of module
Panel Stool Construction	51.60	kg	25% of total module weight
Steel Weight Calculation			
Total hull construction (twin-hull)	9.15	ton	
Total hull construction (monohull)	8.34	ton	

3.2 Governing Equations

The governing equation in the BEM simulation software assumed that the fluid was homogenous, inviscid, irrotational and incompressible as described by Sjøberg and Lund [33] to identify the potential velocity function serves as a criterion for determining fluid characteristics such as velocity and pressure. ANSYS [34] has been utilized to compute RAOs within Boundary Element Method (BEM) techniques. The potential velocity can be written as Eq. (1) with i, j, and k being unit vectors along the x-, y-, and z axes respectively.

$$V = \nabla_{\phi} = \frac{\partial \phi}{\partial x} i + \frac{\partial \phi}{\partial y} j + \frac{\partial \phi}{\partial z} k \tag{1}$$

Within the assumption that the fluid is incompressible, i.e. no change in mass in a flow into and out of control surface, the Laplace equation used the following Eq. (2)

$$\nabla^2 \phi = \frac{\partial u}{\partial x} + \frac{\partial v}{\partial y} + \frac{\partial w}{\partial z} = 0 \tag{2}$$

Subsequently, to satisfy the continuity equation, all potential velocity solutions shall be followed with the non-rotation condition given in Eq. (3). The irrotational fluid is when the vorticity vector is zero everywhere in the fluid.

$$\omega_v = \nabla^2 \times V = 0 \tag{3}$$

Then there will be no flow through the surface of a fixed body in a moving fluid. This condition indicates the body's impermeability and is written as Eq. (4).

$$\frac{\partial \phi}{\partial n} = 0 \tag{4}$$

While Eq. (4) expressed the impermeability of a fixed body, such as the seabed, with n denoting a normal vector pointing from the seabed and out in the fluid, Eq. (5) generalizes the equation for a moving body with a velocity V.

$$\frac{\partial \phi}{\partial n} = V \,.\, n \tag{5}$$

The kinematic free-surface condition explained that under the assumption of small waves, the fluid particles on the surface are supposed to stay on the free surface. Furthermore, the dynamic free-surface condition states that the water pressure on the free surface equals constant atmospheric pressure. The simplified and linearized kinematic and dynamic free-surface conditions can be stated as the following Eq. (6) using linear theory and the assumptions of small waves, zero current, and zero forward speed of the body.

$$\frac{\partial^2 \zeta}{\partial t^2} + g \frac{\partial \phi}{\partial z} = 0 \qquad on \;\; z = 0 \tag{6}$$

Finally, when the vessel interacts with the waves, the potential velocity can be used to express the wave flow field around the hull sections. Furthermore, the potential velocity can be used to calculate the fluid force around the hull section, as well as the hull motion and wave force. As a result, the potential velocity caused by external waves can be superimposed using the following Eq. (7).

$$\phi = \phi_i + \phi_r + \phi_d \tag{7}$$

ϕ_i, ϕ_r, ϕ_d denote the potential functions for the incident wave, radiation wave, and diffraction wave, respectively. ϕ_i computed by utilizing the Airy linear theory, whereas the derivation of ϕ_r and ϕ_d relies on the utilization of the diffraction theory. In diffraction theory, the potential function is determined by solving the Laplace equation, applying the relevant boundary conditions, and subsequently calculating the pressure and the resulting forces acting on the body. Furthermore, the pressure was extracted using the Bernoulli equation while the potential function was determined. In conclusion, the integration of pressure over the complete wet surface area produces wave excitation forces that are then utilized in the AQWA software.

3.3 Response Amplitude Operators (RAOs)

RAOs is a dynamic motion characteristic of a structure induced by waves within a specific frequency range in translation and rotational modes. Translation and rotational RAOs followed by Eq. (8) and Eq. (9).

$$RAO_{(k=x,y,z)} = \frac{\zeta_{k0}}{\zeta_0} \tag{8}$$

$$RAO_{(k=\theta,\phi,\psi)} = \frac{\zeta_{k0}}{\left(\frac{\omega^2}{g}\right)\zeta_0} \tag{9}$$

In 3D panel BEM simulations, Response Amplitude Operator (RAO) data for different types of floating structure motion may be generated in the 0° to 360° range, with 45° increments. It should be noted that the Response Amplitude Operator (RAO) for two degrees of freedom, specifically heaving and pitching, is calculated individually based on the methodologies detailed in previous studies by Tavakoli *et al.,* [35] and Fitriadhy *et al.,* [36]. Waves only arrive from one direction, leading to uncoupled motions as study conducted by Wulandari *et al.,* [37].

3.4 Calculation of Wave Spectral

JONSWAP's wave spectrum formulation is a modified version of the Pierson-Moskowitz spectrum with integrating parameters to accommodate the characteristics of waves in enclosed waters or island environments [31]. Therefore, it is suitable for application in Indonesia's archipelago with the following Eq. (10) to Eq. (14) based on DNV-GL recommendation [38].

$$S_J(\omega) = A_\gamma S_{PM}(\omega)\gamma^{exp\left[-0.5\left(\frac{\omega-\omega_p}{\sigma\omega_p}\right)^2\right]} \tag{10}$$

$$S_{PM}(\omega) = \frac{5}{16}.{H_s}^2{\omega_p}^4.\omega^{-5}exp\left[-\frac{5}{4}\left(\frac{\omega}{\omega_p}\right)^{-4}\right] \tag{11}$$

$$\omega_p = \frac{2\pi}{T_p} \tag{12}$$

$$A_\gamma = 1 - 0.287\ln(\gamma) \tag{13}$$

$$\sigma = 0.07 \text{ for } \omega \leq \omega_p \text{ or } \sigma = 0.09 \text{ for } \omega > \omega_p \tag{14}$$

Where, S_J (ω) is the JONSWAP spectrum, S_{PM} (ω) is the Pierson-Moskowitz spectrum, ω_p is the angular spectral peak frequency, T_p is the spectral peak period, H_s is the significant wave height, A_γ is the normalizing factor, γ is the non-dimensional peak shape parameter, and σ is the spectral width parameter.

3.5 Calculation of Responses Spectral

The responses of a floating structure in irregular waves shall be obtained by correlating the RAO with the wave spectrum within transforming wave energy into response energy with the following Eq. (15). Subsequently, the amplitude significant response is calculated as Eq. (16).

$$S_{\zeta r}(\omega) = RAO^2 \times S_\zeta(\omega) \tag{15}$$

$$\zeta_s = 2\sqrt{m_0} \tag{16}$$

Where $S_{\zeta r}$ (ω) is the response spectrum, S_ζ (ω) is the waves spectrum and m_0 is the area under the response spectrum curve as shown in the following Eq. (17).

$$m_0 = \sum_{n=1}^{\infty} S_\zeta(\omega)\delta\omega = \int_0^\infty S_\zeta(\omega)d\omega \tag{17}$$

3.6 3-D Diffraction BEM Simulation Setup

Maxsurf modeler by Bentley has been used for three-dimensional (3D) models of floating structures [39]. In the next step, the 3D model is exported in a .step (dot step) by utilizing Rhinoceros software to Ansys Aqwa for seakeeping analysis. The statistical validation between Ansys Aqwa and related 3D model software should not exceed of 2% threshold for all considered with the results as shown in Table 4 [40].

Table 4
Statistical validation for both designs

Parameter	Ansys Aqwa		3-D Model Software		Difference (%)	
	Twin-hull	Monohull	Twin-hull	Monohull	Twin-hull	Monohull
Hydrostatic properties						
Displacement Δ (ton)	9.93	9.13	9.96	9.13	0.28	0.00
Water plane area (m^2)	19.31	36.10	19.32	36.00	0.05	0.27
Longitudinal center of gravity, *LCG* (m) from AP	4.49	4.49	4.54	4.55	1.26	1.42
Parameter	Ansys Aqwa		3-D Model Software		Difference (%)	
	Twin-hull	Monohull	Twin-hull	Twin-hull	Monohull	Twin-hull
Inertia properties						
Inertia moment, Ixx ($kg.m^2$)	11563.37	34335.48	11409.19	33816.97	1.33	1.51
Inertia moment, Iyy ($kg.m^2$)	61037.20	57169.20	60264.61	56303.18	1.27	1.51
Inertia moment, Izz ($kg.m^2$)	72566.07	89699.83	71655.47	88367.90	1.25	1.48

As shown in Figure 3, the 3D BEM domain was defined with dimensions as follows [34]:

X = 10 × LOA (90 m), Y = 4.5 × LOA (40.5 m), *Z*= water depth (27 m)

for setting up sea-grid geometry in X, Y, and Z directions.

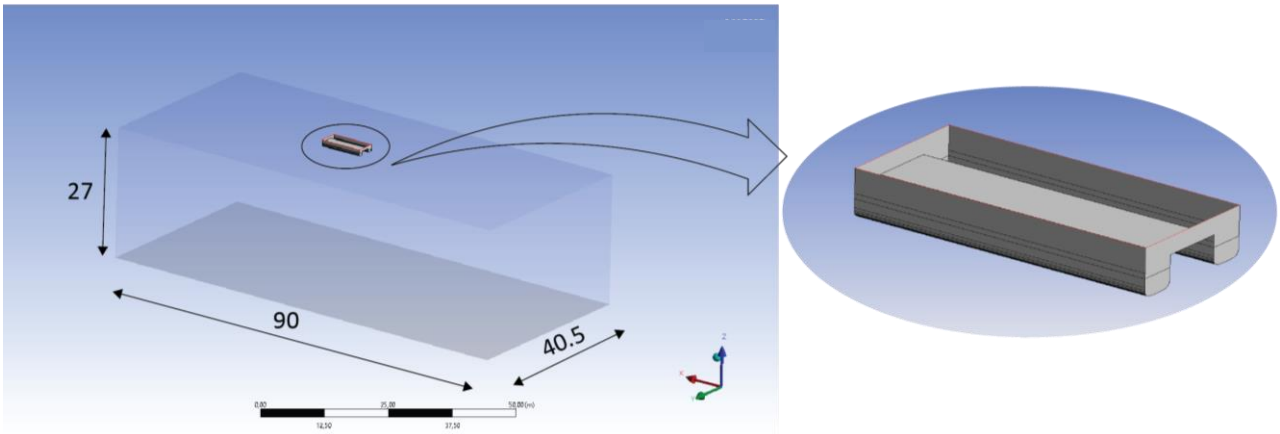

Fig. 3. Computational domain in Ansys Aqwa. Unit in meter

Furthermore, the motion characteristics are the combination of the mass properties and hull surface geometry of the floating structure. The mass properties such as inertia values and centre of gravity (CoG) indicate how resistant a body is to changes in its rotational state. The mass properties are defined in Ansys Aqwa as a “point mass” with automatically calculated in mass and only input in radius gyration as can be seen Table 5.

Table 5
Radii of gyration both of floating structures

Component	Twin-hull (m)	Monohull (m)
k_{xx}	1.079	1.939
k_{yy}	2.479	2.502
k_{zz}	2.703	3.134

The generating mesh provides to calculation of pressures and forces on each number element in hull surface geometry [41]. A finer mesh was used in interface between wet and dry surface region. Both of floating were meshed as shown in Figure 4.

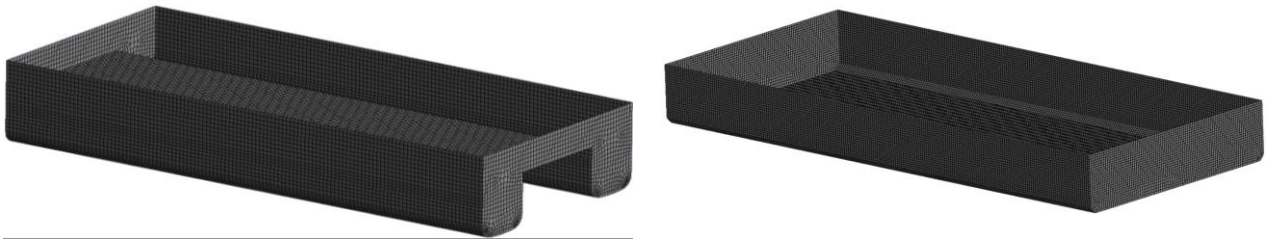

(a) (b)

Fig. 4. Mesh visualization: (a) Twin hull (b) Monohull

4. Grid Independence Test

Grid independence tests were conducted to determine the optimal number of cells (elements) for ensuring convergence in the final numerical simulations. This mesh convergence study was performed to maintain stability and accuracy throughout the computational simulations as stated by Fitriadhy *et al.,* [42]. The area under the RAO curves as a function of the number of elements for heave and roll modes in the heading angle of 90^o will be evaluated with various element sizes both of design. The selection of the optimal mesh size depends on reaches convergence graph in each mode indicating with minimal fluctuation in varying mesh sizes. Figure 5 shows the less than 2% convergence graphs for different varied mesh throughout the 3D BEM simulation within the optimum number of 20,230 elements and 18,456 elements are used for twin-hull and monohull respectively, as shown in the red dashed circle.

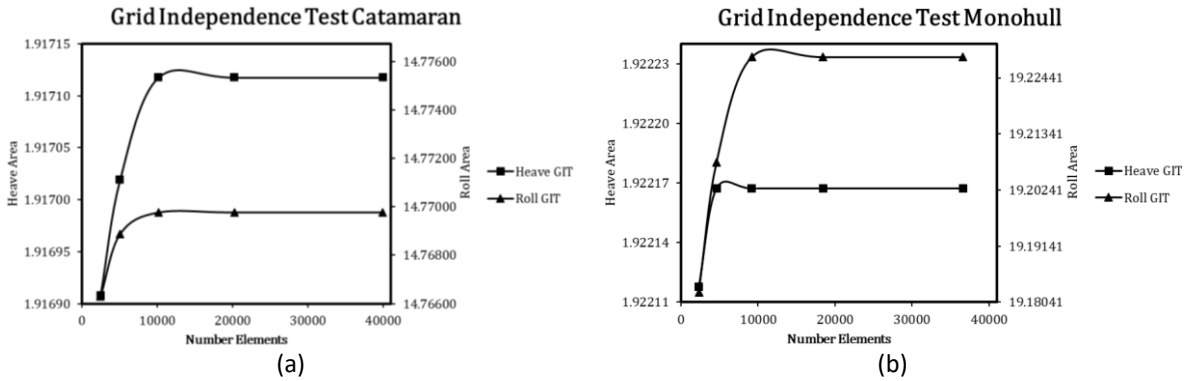

(a) (b)

Fig. 5. The area under RAO curves and function of number element: (a) Twin-hull, (b) Monohull

5. Result and Discussion

The result and discussion in this paper are divided into subsections: Response amplitude operators, wave spectra under various sea states, and response spectra and stochastic values.

5.1 Response Amplitude Operators (RAOs)

The results of seakeeping numerical simulations for both designs are presented in this section. Due to the symmetrical geometry in the stern and bow of both floating structures, the wave heading is considered only in 0º (following sea), 45 º (quartering sea) and 90 º (beam sea). Figure 6 shows the comparison of the effect of hull configuration in heave motion. The largest heave response is for the wave heading 90º, followed subsequently by 45º and 0º. In detail, the monohull model has a lower heave response – but the difference is not too significant – compared to the twin-hull for 0º and 45º, however in 90º for both designs heave response is rather similar to each other.

This aligns with the findings from studies by Kallio and Ricci [43] which indicate that heave motion at a beam sea heading (90°) is greater than at other headings under stationary conditions (Vs = 0 knots), and is smallest under conditions of maximum speed (Vs = 32 knots). Further study conducted by McGibbon and Rizvi [44] investigated that both heave and roll motions are sensitive to beam seas.

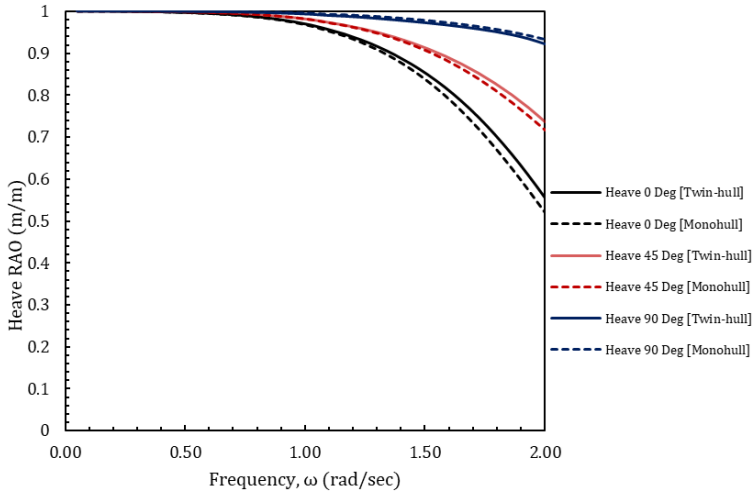

Fig. 6. Heave RAO for both designs hull type

For the roll motion as illustrated in Figure 7, shows that the wave heading in 90º (beam sea) is the dominant rolling motion of the floating structure. The significant difference between each design shows at high wave frequencies (short-wavelength) when the monohull model has a higher motion response than the twin-hull model in all wave headings.

According to a study conducted by Bhattacharya [45], the rolling motion of a twin-hull (catamaran) is also particularly different from that of a conventional monohull, because a twin-hull undoubtedly has a higher value for metacentric height. Thus, twin hulls have lower roll angles, natural rolling periods, lateral accelerations, and high transverse stability.

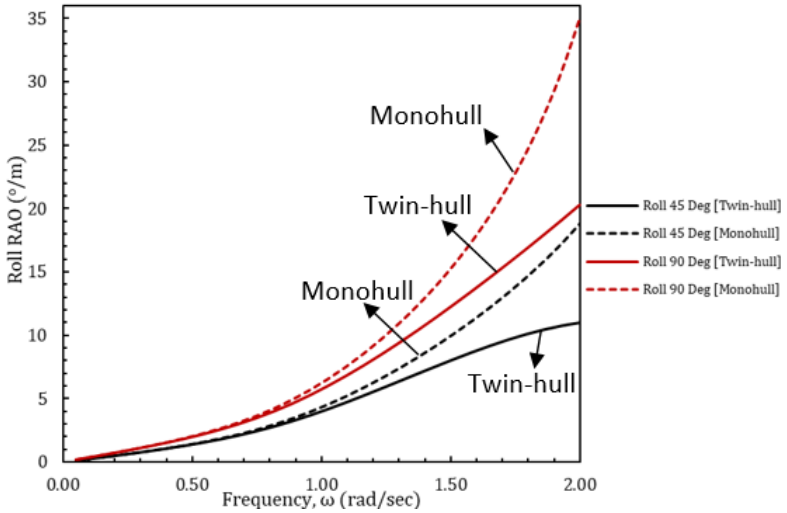

Fig. 7. Roll RAO for both designs hull type

Following with similar pattern to the rolling motion. In pitch motion as presented in Figure 8, the response values for both models significantly increase at high wave frequencies. With the twin-hull design showing slightly higher response values compared to the monohull design. For this case, the dominant wave heading causing the pitch motion is at 0° (following sea).

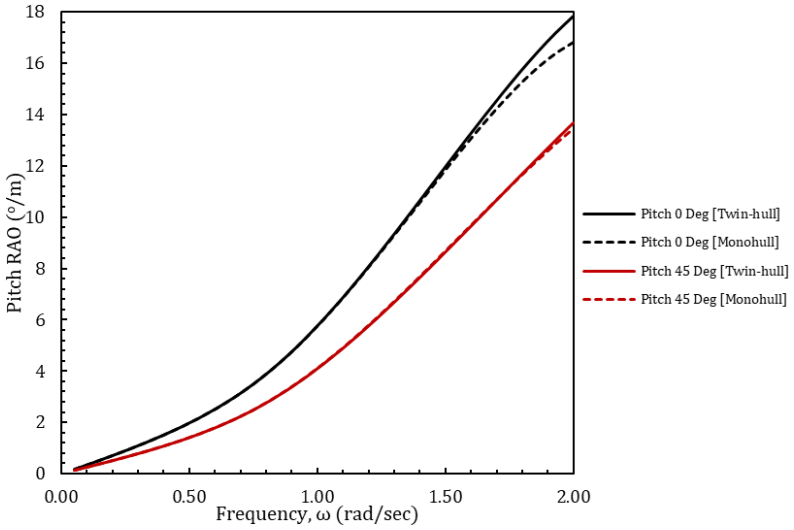

Fig. 8. Pitch RAO for both designs hull type

Upon a closer examination of Figure 6 to Figure 8, which represent various RAO graphs for both models, it becomes clear that each model demonstrated specific advantages in distinct modes. In particular, the monohull design was more reliable in the heave and pitch modes than the twin-hull design, whereas the differences are not significantly apparent.

However, the remarkable aspect lies in the roll RAO, which the twin-hull design convincingly demonstrates its dominance less in motion when compared to the monohull, due to the indication of a lower curve compared to the monohull design, whereas showing a substantial difference of approximately -71.97% at a frequency of 2 rad/sec. Furthermore, the addition of the hull laterally induces a dampening effect on the roll motion, resulting from the increased moment of inertia as weight is concentrated in the two hulls of the catamaran.

5.2 Wave Spectra under Various Sea-State Conditions

The next step for quantifying the effect of the hull configuration is to calculate the wave spectra. Figure 9 shows JONSWAP's wave spectra for sea-state 1 – 4 by following Table 6 which represents sea condition.

The wave spectrum curve graph shows that as the significant wave height increases, it also affects the peak value and energy density within the wave spectrum. Furthermore, this also leads to a shift in the peak value of the wave spectrum curve towards lower frequencies with the following 2.00, 1.58, 1.09, and 0.67 rad/sec for sea-state 1 through 4 respectively.

The relationship can be quantified by observing that the wave height in sea-state 4 is doubled that of sea-state 3. However, the energy density under curve in wave spectrum shows a remarkable increase of approximately 4.37 times.

Table 6
Sea-state codes

Sea-State	Description of sea	Significant Wave Height (m)
1	Calm (rippled)	0.10
2	Smooth (wavelets)	0.50
3	Slight	1.25
4	Moderate	2.50

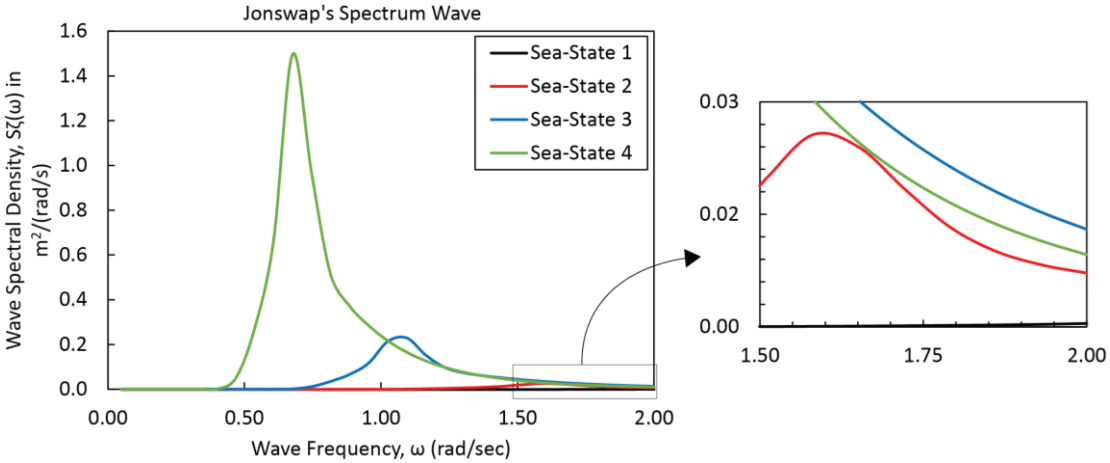

Fig. 9. JONSWAP's spectrum wave for various sea-state

5.3 Response Spectra and Stochastic Value

The calculation of response spectra is influenced by two key parameters: the wave spectrum and RAO in specific modes. As depicted in Figure 10 and Figure 11, the spectral responses in heave and pitch modes for both designs remain relatively minor distinctions in all sea states considered. This observation is following the characteristics of the RAO curves detailed in the previous sub-section. In specific values, for the peak of heave and pitch spectral response in sea-state 4 within wave-frequency of 0.68 rad/sec, the differences between twin-hull and monohull designs are quietly close for 0.08% and 0.02% respectively.

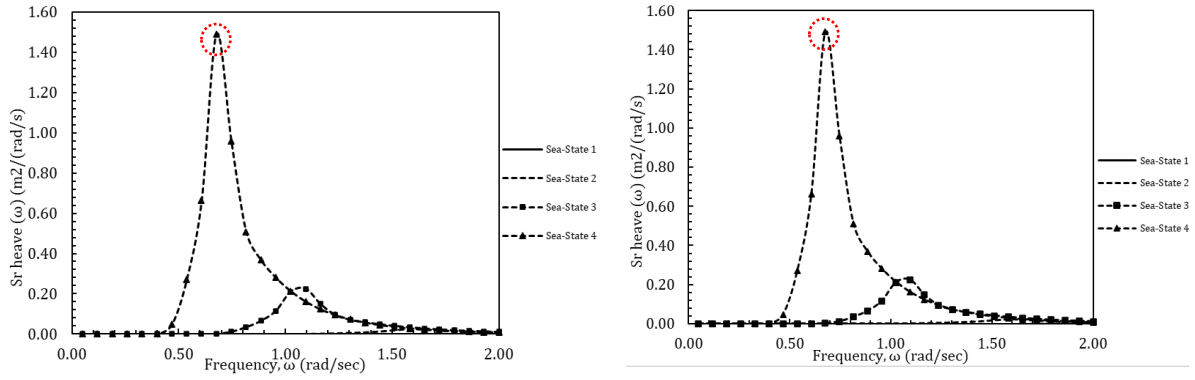

(a) (b)

Fig. 10. Heave response spectra both designs: (a) Twin-hull, (b) Monohull

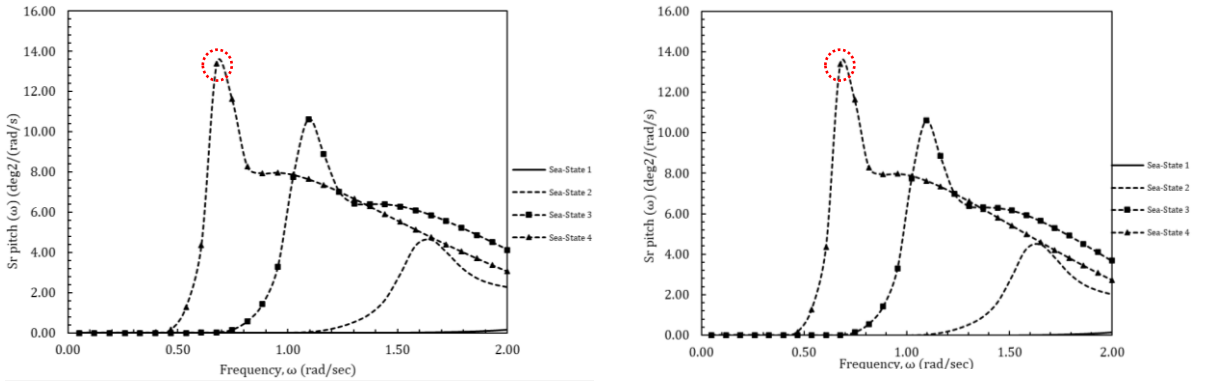

(a) (b)

Fig. 11. Pitch response spectra both designs: (a) Twin-hull, (b) Monohull

However, response characteristics in the roll motion are distinct significantly between the two proposed designs. To be more specific, the twin-hull model has a decrease in spectral response within the frequency range of 1.44 rad/sec to 2 rad/sec for sea-states 3 and 4, whereas the monohull model has an escalation in response behaviour at the same wave frequencies range due to short waves force excitation occur at the beam seas, as indicated by higher values in its RAO curve, with the red dashed box following in the appropriate graph as shown in Figure 12.

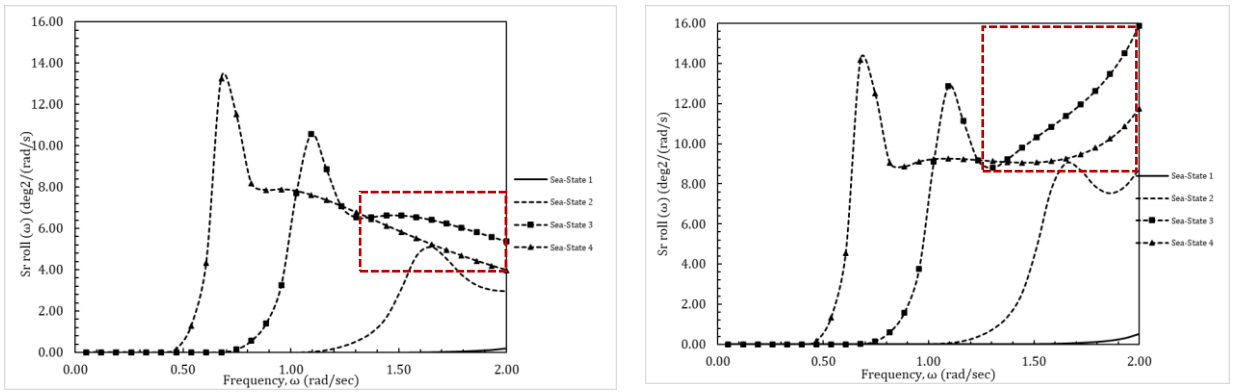

(a) (b)

Fig. 12. Roll response spectra both designs: (a) Twin-hull, (b) Monohull

Furthermore, the stochastic parameters were derived from the response spectra curve from each mode. Nevertheless, for this study, the focus will remain confined to the determination of significant

response amplitudes – an average measurement of the largest 33% of responses – within the range of sea-state 1-4.

In Figure 13, the bar graphs illustrate the significant response values in heave motion indicating a rise response as the wave height increases as the function of sea-state. However, in numerical simulation show that there is no significant differentiation between the two designs. Hence, confidently stated that the significant response heave value in all sea-state is almost identical.

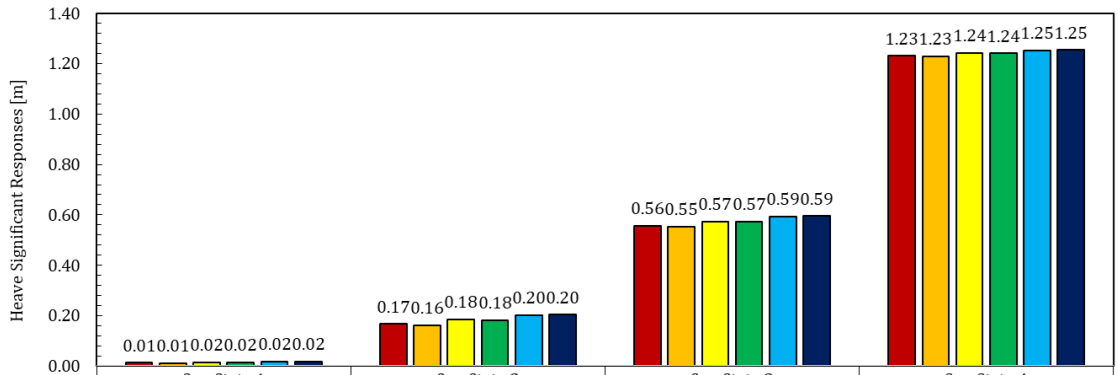

	Sea-State 1	Sea-State 2	Sea-State 3	Sea-State 4
Twin-hull Heading 0 Deg	0.01	0.17	0.56	1.23
Mono Hull Heading 0 Deg	0.01	0.16	0.55	1.23
Twin-hull Heading 45 Deg	0.02	0.18	0.57	1.24
Mono Hull Heading 45 Deg	0.02	0.18	0.57	1.24
Twin-hull Heading 90 Deg	0.02	0.20	0.59	1.25
Mono Hull Heading 90 Deg	0.02	0.20	0.59	1.25

Fig. 13. Heave significant responses

This is similarly reflected in the significant pitch response, as depicted in Figure 14. It reveals that in the dominant pitch heading, the response values are higher compared to the 45°-wave heading. The distinction in pitch motion response between the twin-hull and monohull design models are 3.3%, 2.5%, 1.2%, and 0.7% for sea states 1 through 4, respectively. However, in wave heading 45°, the pitch response remains identical throughout all sea states.

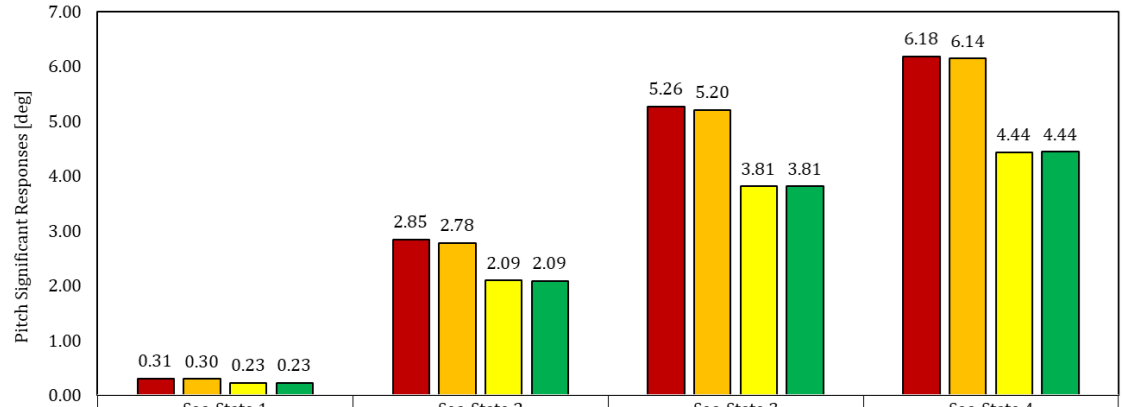

	Sea-State 1	Sea-State 2	Sea-State 3	Sea-State 4
Twin-hull Heading 0 Deg	0.31	2.85	5.26	6.18
Mono Hull Heading 0 Deg	0.30	2.78	5.20	6.14
Twin-hull Heading 45 Deg	0.23	2.09	3.81	4.44
Mono Hull Heading 45 Deg	0.23	2.09	3.81	4.44

Fig. 14. Pitch significant responses

The significant roll response has a more substantial effect. This specific response significantly leads to a strong differentiation between the two designs. As illustrated in Figure 15, the difference in response values in prevailing 90°-roll heading stands at 53%, 39%, 27%, and 18% for sea states 1

through 4, respectively. Subsequently in 45° wave-heading (quartering sea) it demonstrates a slightly lower disparity compared to the 90° wave-heading (beam sea) through sea-state 1-4 stand for 50%, 37%, 24% and 16% respectively.

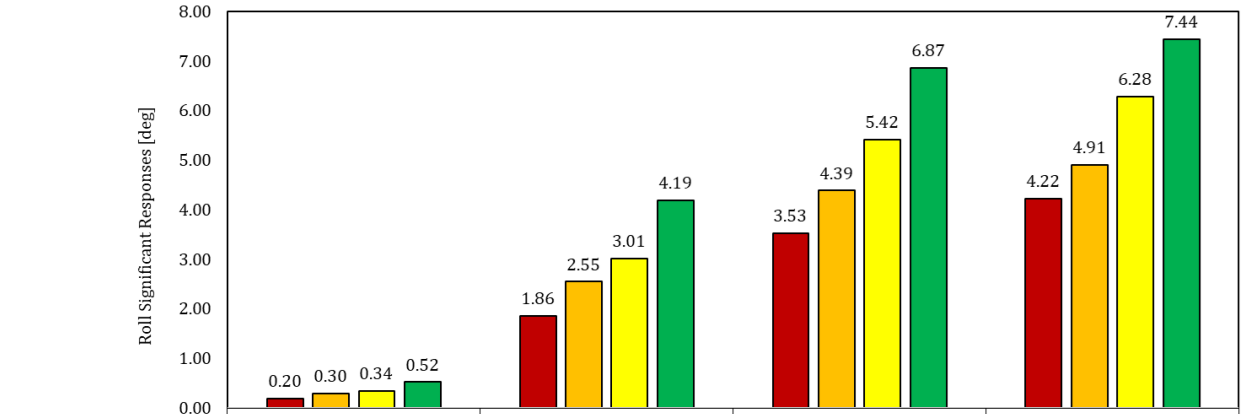

	Sea-State 1	Sea-State 2	Sea-State 3	Sea-State 4
Twin-hull Heading 45 Deg	0.20	1.86	3.53	4.22
Mono Hull Heading 45 Deg	0.30	2.55	4.39	4.91
Twin-hull Heading 90 Deg	0.34	3.01	5.42	6.28
Mono Hull Heading 90 Deg	0.52	4.19	6.87	7.44

Fig. 15. Roll significant responses

Figure 13 to Figure 15 make an interesting observation. The bar graph patterns for heave and pitch responses indicate only slight differences between the two design approaches. However, a significant discrepancy appears in the case of roll motion, when the disparities rise above 1.5 times, specifically in sea state 1.

6. Conclusions

A study into the effect of hull configuration on seakeeping characteristics of floating photovoltaic systems has been investigated. Numerical BEM with Green-Function simulations based on 3-D diffraction were conducted to identify pure oscillatory motions in heave, pitch, and roll. The simulation results show that the twin-hull model has more advantages than the monohull design. The trend of the RAO pattern, response spectra, and significant response for heave and pitch motion represent only slight differences between the two proposed designs. However, substantial disparity emerges in roll motion, with the difference in response values in prevailing 0° -roll heading standing at 53%, 39%, 27%, and 18% for sea states 1 through 4, respectively. Moreover, in 45° wave-heading (quartering sea) demonstrates a slightly lower disparity compared to the 0° wave-heading (following sea) through sea-state 1-4 standing for 50%, 37%, 24% and 16% respectively.

The focus of future design optimization will be on enhancing the hull configuration and selecting appropriate materials. The goal is to create a floater model that is both affordable and resilient, particularly in challenging environments. Additionally, as FPV technology continues to evolve, it is expected to move towards the concept of energy farming at sea. This will involve evaluating various configurations on the water surface within the mooring design model, considering their hydrodynamic response through time domain analysis.

Acknowledgement
The authors would like to express their gratitude to the Ministry of Education, Culture, Research, and Technology of the Republic of Indonesia for funding this research under the “Master Program of

Education Leading to a Doctoral Degree for Excellent Graduates (PMDSU) Batch VII," through Grant Number 038/E5/PG.02.00.PL/2024 and local Grant Number 1797/PKS/ITS/2024. The authors also acknowledge that this research was partly funded by the Innovate UK "Solar2Wave" project, under Grant Number 10048187.

References

[1] Directorate General of Renewable Energy and Energy Conservation. *Performance Report of the Directorate General of Renewable Energy and Energy Conservation for 2022*. Jakarta: EBTKE Directorate General, 2022.
[2] Indonesia State Electricity Company. *Electricity Supply Business Plan (RUPTL) 2021-2030*. Jakarta: State Electricity Company (PT PLN), 2021.
[3] Trapani, Kim, and Miguel Redón Santafé. "A review of floating photovoltaic installations: 2007-2013." *Progress in Photovoltaics: Research and Applications* 23, no. 4 (2015): 524-532. https://doi.org/10.1002/pip.2466
[4] Lee, Nathan, Ursula Grunwald, Evan Rosenlieb, Heather Mirletz, Alexandra Aznar, Robert Spencer, and Sadie Cox. "Hybrid floating solar photovoltaics-hydropower systems: Benefits and global assessment of technical potential." *Renewable Energy* 162 (2020): 1415-1427. https://doi.org/10.1016/j.renene.2020.08.080
[5] Cazzaniga, Raniero, M. Cicu, Marco Rosa-Clot, P. Rosa-Clot, G. M. Tina, and C. Ventura. "Floating photovoltaic plants: Performance analysis and design solutions." *Renewable and Sustainable Energy Reviews* 81 (2018): 1730-1741. https://doi.org/10.1016/j.rser.2017.05.269
[6] World Bank Group, ESMAP and SERIS. *Where Sun Meets Water: Floating Solar Handbook for Practitioners*. World Bank Group, Washington, DC, 2019.
[7] Det Norske Veritas. *Recommended Practice: Design, Development and Operation of Floating Solar Photovoltaic Systems*. DNVGL-RP-0584, 2021.
[8] Ramasamy, Vignesh, and Robert Margolis. *Floating photovoltaic system cost benchmark: Q1 2021 installations on artificial water bodies*. No. NREL/TP-7A40-80695. National Renewable Energy Lab.(NREL), Golden, CO (United States), 2021. https://doi.org/10.2172/1828287
[9] Masdar. "Cirata Floating Photovoltaic (FPV) Plant." *Masdar*, 2023.
[10] Reuters. "Sunseap to Build $2 Billion Floating Solar Farm in Indonesia, World's Largest." *Reuters*. July 22, 2021.
[11] Institute for Essential Services Reform (IESR). *Technical Potential of Floating Solar Photovoltaic in Central Java*. IESR, 2021.
[12] Joshi, Prateek, Evan Rosenlieb, and Sika Gadzanku. *Enabling Floating Solar Photovoltaic (FPV) Deployment: FPV Technical Potential Assessment for Southeast Asia*. No. NREL/TP-5R00-84921. National Renewable Energy Laboratory (NREL), Golden, CO (United States), 2023. https://doi.org/10.2172/1974575
[13] Ardiansyah, Harun, and Putty Ekadewi, eds. *Indonesia Post-Pandemic Outlook: Strategy towards Net-Zero Emissions by 2060 from the Renewables and Carbon-Neutral Energy Perspectives*. Penerbit BRIN, 2022.
[14] Sahu, Alok K., and Kumarasamy Sudhakar. "Effect of UV exposure on bimodal HDPE floats for floating solar application." *Journal of Materials Research and Technology* 8, no. 1 (2019): 147-156. https://doi.org/10.1016/j.jmrt.2017.10.002
[15] Mittal, Divya, Bharat Kumar Saxena, and K. V. S. Rao. "Floating solar photovoltaic systems: An overview and their feasibility at Kota in Rajasthan." In *2017 International Conference on Circuit, Power and Computing Technologies (ICCPCT)*, pp. 1-7. IEEE, 2017. https://doi.org/10.1109/ICCPCT.2017.8074182
[16] Cazzaniga, R., M. Cicu, M. Rosa-Clot, P. Rosa-Clot, G. M. Tina, and C. Ventura. "Compressed air energy storage integrated with floating photovoltaic plant." *Journal of Energy Storage* 13 (2017): 48-57. https://doi.org/10.1016/j.est.2017.06.006
[17] Rosa-Clot, Marco, and Giuseppe Marco Tina. "Chapter 5 - The Floating PV Plant." *Submerged and Floating Photovoltaic Systems: Modelling, Design and Case Studies* (2018): 89-136. https://doi.org/10.1016/B978-0-12-812149-8.00005-3
[18] Sigtryggsdottir, Fjola Gudrun. *Environmental Loads on Embankment in Mountainous Regions*. NVE Ekstern rapport nr. 16/2022, 2022.
[19] Pullen, Tim, William Allsop, Eunice Silva, Craig Goff, and Tracey Williamson. "Wave and overtopping predictions on reservoirs and inland waterways." In *3rd International Conference on Protection against Overtopping*, pp. 6-8 June 2018. 2018.
[20] Wang, Zhiwen, Rupp Carriveau, David S-K. Ting, Wei Xiong, and Zuwen Wang. "A review of marine renewable energy storage." *International Journal of Energy Research* 43, no. 12 (2019): 6108-6150. https://doi.org/10.1002/er.4444

[21] Kit, Andrew Yip Jun, Sunny Goh Eng Giap, and Mohammad Fadhli Ahmad. "Experimental Study on Wave Transmission Coefficient of Double Cylindrical Floating Breakwater in a Wave Basin." *Journal of Advanced Research in Fluid Mechanics and Thermal Sciences* 112, no. 2 (2023): 33-42. https://doi.org/10.37934/arfmts.112.2.3342
[22] Liu, Haohui, Vijay Krishna, Jason Lun Leung, Thomas Reindl, and Lu Zhao. "Field experience and performance analysis of floating PV technologies in the tropics." *Progress in Photovoltaics: Research and Applications* 26, no. 12 (2018): 957-967. https://doi.org/10.1002/pip.3039
[23] Ahmed, Mushtaq, Zafarullah Nizamani, Akihiko Nakayama, and Montasir Osman. "Some Recent Fluid-Structure Interaction Approaches for the Wave Current Behaviour With Offshore Structures." *CFD Letters* 12, no. 9 (2020): 15-26. https://doi.org/10.37934/cfdl.12.9.1526
[24] Andrady, Anthony L. "Microplastics in the marine environment." *Marine Pollution Bulletin* 62, no. 8 (2011): 1596-1605. https://doi.org/10.1016/j.marpolbul.2011.05.030
[25] Ciel & Terre International. "Hydrelio® Floating solar photovoltaic panels for water resource conservation." *Solar Impulse Foundation*, 2020.
[26] Oliveira-Pinto, Sara, and Jasper Stokkermans. "Marine floating solar plants: An overview of potential, challenges and feasibility." In *Proceedings of the Institution of Civil Engineers-Maritime Engineering*, vol. 173, no. 4, pp. 120-135. Thomas Telford Ltd, 2020. https://doi.org/10.1680/jmaen.2020.10
[27] CSI Solar. "Preliminary Technical Sheet of Canadian Solar." *CSI Solar Co., Ltd*., 2021.
[28] Insel, Musatafa, and A. F. Molland. *An Investigation into the Resistance Components of High Speed Displacement Catamarans*. The Royal Institution of Naval Architects, 1992.
[29] Watson, D. G. M. *Practical ship design*. Elsevier, 1998.
[30] Lewis, Edward V. *Principles of naval architecture*. Society of Naval Architects & Marine Engineers, 1988.
[31] Djatmiko, Eko Budi. *Behavior and Operability of Ocean Structure on Random Waves*, ITS Press, 2012.
[32] Directorate General of Renewable Energy and Energy Conservation. *Centralized Solar Power Plant Feasibility Study Guidelines*. Jakarta: EBTKE Directorate General, 2018.
[33] Sjøberg, Trym Sogge, and Øyvind Haug Lund. "Evaluation and Comparison of Operability and Operational Limits of Service Vessel Designs in Exposed Aquaculture." *Master's thesis, NTNU*, 2018.
[34] ANSYS. "Ansys Aqwa Theory Manual." *ANSYS Inc., Canonsburg*, 2012.
[35] Tavakoli, Sasan, Rasul Niazmand Bilandi, Simone Mancini, Fabio De Luca, and Abbas Dashtimanesh. "Dynamic of a planing hull in regular waves: Comparison of experimental, numerical and mathematical methods." *Ocean Engineering* 217 (2020): 107959. https://doi.org/10.1016/j.oceaneng.2020.107959
[36] Fitriadhy, Ahmad, Syarifuddin Dewa, Nurul Aqilah Mansor, Nur Amira Adam, Cheng Yee Ng, and Hooi Siang Kang. "CFD investigation into seakeeping performance of a training ship." *CFD Letters* 13, no. 1 (2021): 19-32. https://doi.org/10.37934/cfdl.13.1.1932
[37] Wulandari, Amalia Ika, I Ketut Aria Pria Utama, Afifah Rofidayanti, and Dominic Hudson. "Numerical Analysis of Ship Motion of Crew Boat with Variations of Wave Period on Ship Operational Speed." *CFD Letters* 16, no. 4 (2024): 1-15. https://doi.org/10.37934/cfdl.16.4.115
[38] Det Norske Veritas. *Recommended Practice Environmental Conditions and Environmental Loads*. DNV-RP-C205, 2010.
[39] Couser, Pat. "MAXSURF Manuals." *Bentley*, 2022.
[40] Suastika, Ketut, Agung Silaen, Muhammad Hafiz Nurwahyu Aliffrananda, and Yuda Apri Hermawan. "Seakeeping analysis of a hydrofoil supported watercraft (hysuwac): A Case Study." *CFD Letters* 13, no. 5 (2021): 10-27. https://doi.org/10.37934/cfdl.13.5.1027
[41] Bosma, Bret, Zhe Zhang, Ted K. A. Brekken, H. Tuba Özkan-Haller, Cameron McNatt, and Solomon C. Yim. "Wave energy converter modeling in the frequency domain: A design guide." In *2012 IEEE Energy Conversion Congress and Exposition (ECCE)*, pp. 2099-2106. IEEE, 2012. https://doi.org/10.1109/ECCE.2012.6342553
[42] Fitriadhy, Ahmad, Nur Amira Adam, Nurul Aqilah Mansor, Mohammad Fadhli Ahmad, Ahmad Jusoh, Noraieni Hj Mokhtar, and Mohd Sofiyan Sulaiman. "CFD Investigation into The Effect of Heave Plate on Vertical Motion Responses of a Floating Jetty." *CFD Letters* 12, no. 5 (2020): 24-35. https://doi.org/10.37934/cfdl.12.5.2435
[43] Kallio, J. A., and J. J. Ricci. *Seaworthiness Characteristics of a Small Waterplane Area Twin Hull (SWATH IV). PART II*. No. SPD-620-02-Pt2. 1976.
[44] McGibbon, Christopher Lewis, and Md Jahir Rizvi. "Effects of nearshore wave reflections on the behaviour of an axe bow trimaran hull." *Ship Technology Research* 68, no. 3 (2021): 179-188. https://doi.org/10.1080/09377255.2021.1892906
[45] Bhattacharyya, Rameswar. *Dynamics of marine vehicles*. Wiley, 1978.